Contents lists available at ScienceDirect

Chemical Physics Letters

journal homepage: http://ees.elsevier.com

Research paper

Heterogeneous kinetics of photoinduced cross-linking of silica nanoparticles with surface-tethered anthracenes

Seyed Hossein Mostafavi [a], Magi Mettry [b], Adam David Gill [c], Connor J. Easley [b], Richard J. Hooley [b,c], Christopher J. Bardeen [b,d]

[a] Department of Bioengineering, University of California, Riverside, Riverside, CA 92521, United states
[b] Department of Chemistry, University of California, Riverside, Riverside, CA 92521, United states
[c] Department of Biochemistry and Molecular Biology, University of California, Riverside, Riverside, CA 92521, United states
[d] Materials Science and Engineering, University of California, Riverside, Riverside, CA, United states

ABSTRACT

Anthracene (**AN**) attachment to silica nanoparticles leads to multiple fluorescence lifetimes, due to different environments on the silica surface. Under ultraviolet (365 nm) illumination, the **AN** surface groups undergo a [4 + 4] photodimerization reaction that cross-links the nanoparticles and induces aggregation. The kinetics of both intra- and inter-particle photochemical reactions are measured by monitoring changes in the surface-bound **AN** absorbance at different nanoparticle concentrations. Our results confirm that the **AN** photodimerization reaction can be used to cross-link silica NPs but also suggest that silica's chemical heterogeneity enables competing reactions that reduce the efficiency of the photochemical cross-linking.

1. Introduction

Materials that can reconfigure themselves after exposure to an external stimulus have potential applications as sensors and actuators [1]. The external stimulus can be chemical (e.g. a pH change), or physical, such as heat or the application of a magnetic field. Light is a particularly useful stimulus because it does not change the chemical composition, does not require physical contact, and has multiple degrees of freedom (intensity, polarization, and wavelength) that can be used as control parameters. One strategy to make photoresponsive materials is to surround nanoparticles (NPs) with organic molecules that can undergo photochemical reactions, for example [2 + 2] and [4 + 4] photodimerizations that create covalent cross-links between NPs [2–10], or photoisomerization reactions that change the surface properties and lead to NP aggregation [11–18].

Previous experimental work has mostly concentrated on metal or polymer NPs whose surfaces are relatively homogeneous. Less attention has been paid to oxide NPs, but this class of materials is potentially more useful. In particular, SiO_2 can be used as an inert yet porous shell to enclose different types of cores that support a wide variety of functionalities, from plasmonic to magnetic to catalytic [19,20]. A general way to stitch together silica-coated NPs could provide a route to new types of photocontrolled, multifunctional nanomaterials.

In the present work, we examine the ability of silica NPs decorated at the surface with anthracenes (**AN**s) to undergo photoinduced self-assembly. The anthracene [4 + 4] photodimerization provides a robust, spectroscopically accessible cross-linking reaction that has been successfully used to assemble gold NPs [21,22]. Our goal is to quantitatively characterize the surface coverage and cross-linking kinetics in order to develop a quantitative kinetic model that takes both intra- and interparticle reactions into account. Analysis of the extracted rate constants allows us to assess how heterogeneity leads to different types of **AN** photochemical reactions that compete with the desired cross-linking reaction. The results in this Letter confirm that surface conjugated **AN**s can be used to cross-link silica NPs, but also highlight heterogeneous behavior that likely results from a diversity of NP surface sites. This heterogeneity may complicate efforts to develop NP systems that can be rapidly reconfigured in a reproducible manner.

2. Experimental

2.1. Synthesis of 9-anthracene-carboxylic acid- N-hydroxysuccinimidyl ester

In a 250 mL round bottle flask equipped with magnetic stir bar was added 9-Anthracenecarboxylic acid (2.0 g, 8.9 mmol) and N-hydroxysuccinimide (1.2 g, 10.8 mmol) in 4 mL of dry dichloromethane. The reaction was stirred for 15 min at 0 °C under N_2 atmosphere followed by slow addition of N, N'-dicyclohexylcarbodiimide (DCC) (1.9 g, 8.9 mmol) to the mixture. After complete addition, the reaction was stirred for 4 hr at 0 °C. Excess DCC was removed by vacuum filtration through a short silica plug and the dichloromethane layer was concen-

E-mail addresses: richard.hooley@ucr.edu (R.J. Hooley); christopher.bardeen@ucr.edu (C.J. Bardeen)

https://doi.org/10.1016/j.cplett.2019.137059
Received 25 September 2019; Received in revised form 5 December 2019; Accepted 21 December 2019
Available online xxx
0009-2614/

trated by rotary evaporation. The crude product was recrystallized in toluene. Finally, the product was purified *via* silica column eluted by dichloromethane to yield pure white product (2.5 g, 88%). ^{1}H NMR (400 MHz, $CDCl_3$) δ 8.63 (s, 1H), 8.41 (dt, J = 8.8, 1.0 Hz, 2H), 8.04 (d, J = 8.5 Hz, 2H), 7.64 (ddd, J = 9.0, 6.6, 1.3 Hz, 2H), 7.53 (ddd, J = 7.9, 6.6, 1.1 Hz, 2H), 3.37–2.70 (m, 4H). ^{13}C NMR (126 MHz, $CDCl_3$) δ 169.38, 165.00, 131.46, 130.68, 129.55, 128.56, 128.15, 125.88, 124.88, 121.34, 25.91. ESI-MS: m/z $C_{19}H_{14}NO_4$ (MH^+) calculated = 320.0918, found: $[MH]^+$ = 320.9090.

Anthracene attachment to silica nanoparticles. 3-aminopropyl functionalized silica NPs [23], suspended in ethanol, were purchased from Sigma-Aldrich (catalog number 660442). 1 mL of this suspension was mixed with 2 mL of anhydrous ethanol and 2 mL of dry dichloromethane, and then 10.8 mg of the 9-anthracene-carboxylic acid-N-hydroxysuccinimidyl ester linker was added to the solution. The mixture was sonicated for 1 min and then gently stirred for 24 h at 35 °C. After completion, the reaction mixture was centrifuged at the speed of 13,000 rpm for 30 min. The supernatant was discarded and the pellet resuspended in anhydrous ethanol and centrifuged again. The procedure was repeated 4–5 times, until no trace of the **AN** linker absorption could be detected in the supernatant. The anthracene coverage was calculated using absorption spectroscopy.

Photoinduced NP aggregation. Various concentrations of the **AN**-SiO_2 NPs were irradiated in a 1 cm pathlength quartz cuvette using a 365 nm lamp source with an intensity of 2.5 mW/cm^2. The absorbance was measured at various time intervals using a Cary 500 spectrophotometer.

Characterization. The **AN**-SiO_2 NPs were characterized using scanning electron microscopy (SEM) with a NovaNanoSEM 450 scanning electron microscope. The dried samples were coated with a thin layer of palladium using a Cressington 108 sputter coater. Dynamic Light Scattering (DLS) and zeta potential measurements were performed using a Malvern ZetaSizer instrument. The **AN**-SiO_2 NPs were sonicated for 10 min to disperse them before injection into the ZetaSizer instrument. Time-resolved photoluminescence measurements were done using 400 nm femtosecond pulses at a 1 kHz repetition rate. The 400 nm excitation wavelength was generated by using a Beta Barium Borate crystal to frequency double the 800 nm fundamental of a Coherent Libra regeneratively amplified Ti:sapphire laser system. The sample was degassed using by bubbling argon gas through it and the fluorescence was collected using front-face detection and a Hanamatsu C4334 streak camera with a time resolution of 25 ps and a wavelength resolution of 2 nm.

3. Results and discussion

The procedure for preparing anthracene (**AN**) functionalized SiO_2 NPs is shown in Scheme 1 [24,25]. The small diameter (~20 nm) of the NPs allowed the absorption spectrum of the suspension to be measured with a low scattering background (Fig. 1). The vibronic lineshape of the **AN**-SiO_2 NPs was similar to that of 9-anthracenecarboxylic acid and the unreacted linker, indicating that the proximity of the SiO_2 does not strongly perturb the electronic structure of the aromatic core. The absorption coefficient of the linker was determined to be ε(365 nm) = 6900 $M^{-1}cm^{-1}$, allowing us to estimate the effective concentration of **AN** in the suspension from the absorption. Since the total mass of SiO_2 NPs in the suspension was also measured, we could calculate that there were 1100 ± 200 **AN** molecules per each NP. Given a NP diameter of 20 nm, this corresponds to a surface coverage of 0.8 ± 0.1 **AN**/nm^2, which is within the measured range of amine coverage on silica NPs [23,26].

The presence of the tethered **AN** molecules affected the NP surface charge, as expected. Measurements of zeta potential showed a change from −30 mV for bare SiO_2 NPs to 6.2 ± 0.5 mV for the amine-terminated SiO_2 NPs and then to 11.4 ± 1.24 mV for the SiO_2-AN NPs. This increase in the NP zeta potential is typically seen when the negatively charged siloxy surface groups are replaced by amines and then by tethered anthracenes [27,28]. The loss of surface negative charge is accompanied by a tendency to aggregate. Dynamic light scattering measurements showed that the average particle size in the suspension was 55 ± 2 nm for the SiO_2-NH_2 sample and 158 ± 7 nm for the **AN**-SiO_2 sample, suggesting that the NPs were slightly aggregated even before any photochemistry occurred. The An-SiO_2 NP suspension was stable in the absence of light for more than one week, exhibiting no change in absorbance or precipitation.

Fig. 2 shows the fluorescence decays for the **AN**-linker in ethanol solution and for the **AN**-SiO_2 NPs. In solution the **AN**-linker exhibited a single exponential decay with a lifetime of 3.2 ± 0.2 ns, identical to that measured for 9-anthracenecarboxylic acid in

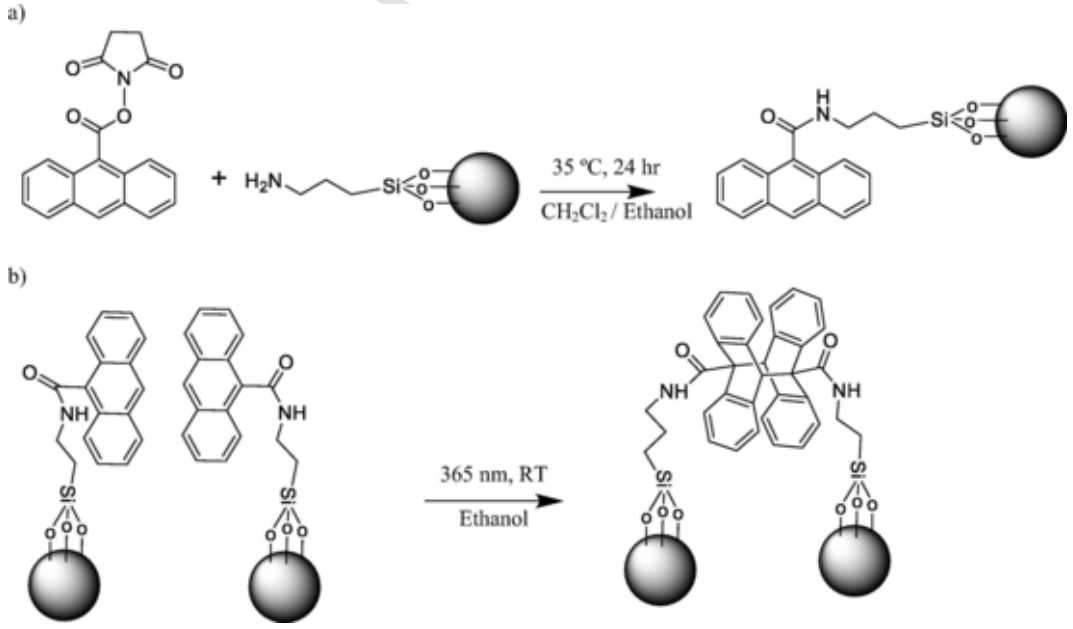

Scheme 1. (a) Method of attaching **AN** to surface of propylamine-terminated SiO_2 NPs. (b) Photodimerization reaction conditions used for crosslinking the **AN**-SiO_2 NPs.

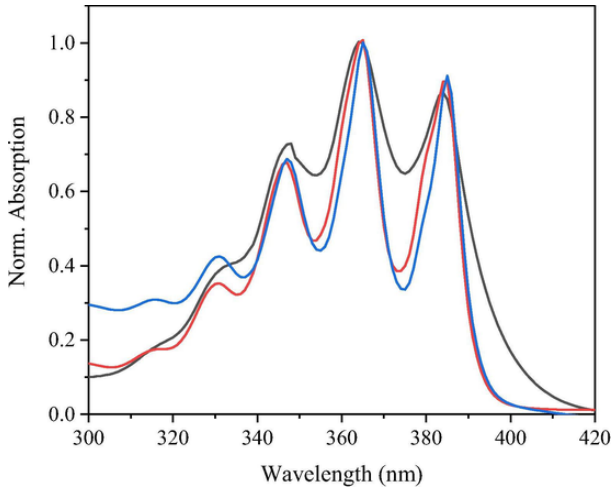

Fig. 1. Normalized absorption spectra of the **AN** linker (black), 9 anthracene carboxylic acid (red) and the **AN**-SiO2 NPs (blue). The peaks and overall lineshapes of the three different anthracene moieties are similar, suggesting that the SiO_2 does not perturb the electronic structure of the aromatic core of the anthracene.

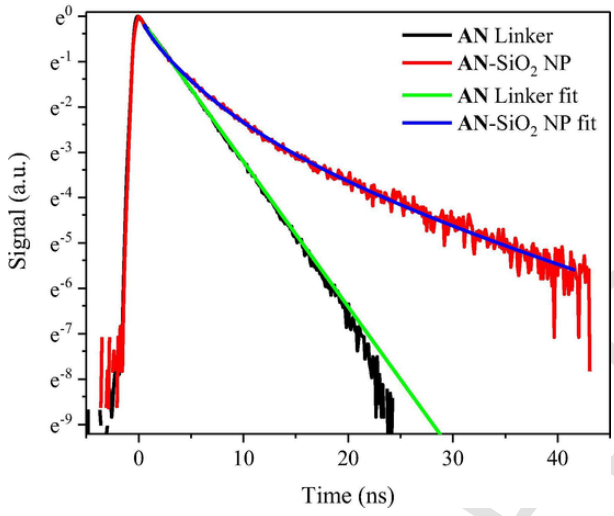

Fig. 2. Time-resolved fluorescence measurements of the **AN** linker (black) and the **AN**-SiO_2 NPs (red) in ethanol. The **AN** linker decay can be fit with a single exponential with a lifetime of 3.2 ± 0.2 ns (green) but the **AN**-SiO_2 decay must be fit with a biexponential decay with lifetimes of 1.2 ns and 7.1 ns. (For interpretation of the references to colour in this figure legend, the reader is referred to the web version of this article.)

ethanol (3.1 ± 0.1 ns). When bound to the NP surface, the **AN** fluorescence decay could only be fit using a biexponential function of the form $Aexp\left[-\frac{t}{\tau_A}\right] + Bexp\left[-\frac{t}{\tau_B}\right]$. The fit, overlaid with the data in Fig. 2, yields τ_A = 1.2 ns and τ_B = 7.1 ns, with the amplitude ratio A/B = 4.1. Note that this decay has both shorter and longer components than observed for the linker in solution. There is no change in the fluorescence spectrum over the course of this decay (Supporting Information, Fig. S3) so it must be attributed to surface-bound **AN** molecules that experience different nonradiative decay rates, presumably due to different local environments. This effect of the SiO_2 surface on the fluorescence decay has been observed for other molecules and has been taken as evidence for the heterogeneity of the SiO_2 surface [29–31].

Given the spectroscopic evidence for different **AN** environments on the NP surface, it was important to determine whether this heterogeneity is also reflected in the cross-linking kinetics. When a suspension of NPs was exposed to 365 nm UV light, the particles agglomerated and the larger masses slowly fell out of suspension, as shown in Fig. 3a. The resulting suspension can be deposited on a glass slide, dried, and examined using SEM (Fig. 3b and 3c). Before UV irradiation, the NPs spread evenly across the glass surface. After UV irradiation, large clumps of NPs were visible, the result of NPs becoming attached together in the suspension. We confirmed that the NP cross-linking requires the attached **AN** molecules, since no photoinduced agglomeration was observed for amine terminated NPs by themselves. It would have been desirable to obtain more definitive evidence of **AN** photodimer formation using an independent analytical measurement. Unfortunately, nuclear magnetic resonance experiments on **AN**-SiO_2 samples that had been dissolved in base and extracted with $CHCl_3$ yielded a spectrum reflecting a complex mixture of species.

The progress of the cross-linking reaction can be followed by monitoring the disappearance of the **AN** absorption, since the loss of conjugation in the photodimer shifts its absorbance into the UV region. But to extract accurate rate information, it is important to use samples that are optically thin. Highly absorbing samples suffer from nonuniform illumination due to light attenuation, and this effect evolves as the absorbance falls during the course of the reaction. For all experiments, the peak absorbance was kept below 0.15 in order to minimize such inner filter effects. The initial concentration of NPs (all with the same **AN** surface coverage) could varied, leading to different effective initial **AN** concentrations, but in this case different path-length cells had to be used to keep the initial absorbance low. Before every measurement, the sample was vigorously stirred to make sure there was a homogeneous distribution of NPs in the sample area.

In Fig. 4, we show an example of the decay of a sample with an initial **AN** concentration $N(0)$ = 0.138 mM. After four hours of exposure to 365 nm, the **AN** absorbance has completely vanished. We can plot the absorbance (measured for the largest peak at 381 nm) versus time, and these normalized data are shown in Fig. 5 for two different **AN** initial concentrations, $N(0)$ = 0.138 mM and $N(0)$ = 0.012 mM. The NP decays are non-exponential, with a rapid initial decline followed by a slower component. The rate of absorption loss is concentration de-

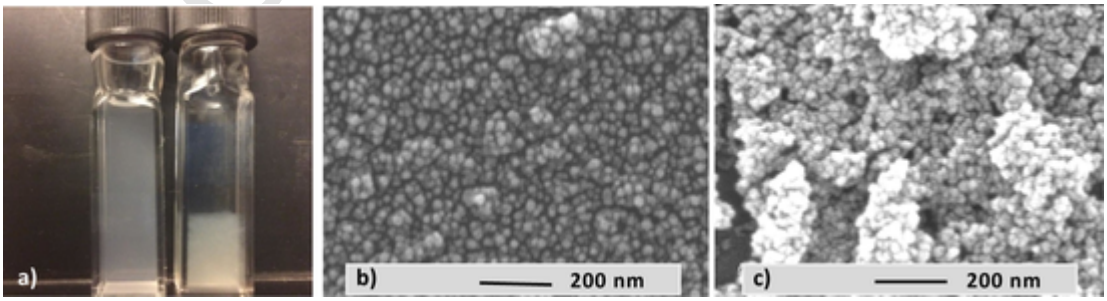

Fig. 3. (a) Cuvette containing an ethanol suspension of **AN**-SiO_2 NPs before (left) and after (right) 3 h of 365 nm irradiation that causes the NPs to agglomerate and fall to the bottom of the cuvette. (b) Scanning electron microscopy (SEM) image showing a layer of NPs before 365 nm exposure. (c) SEM image showing the formation of large NP clusters after 365 nm exposure.

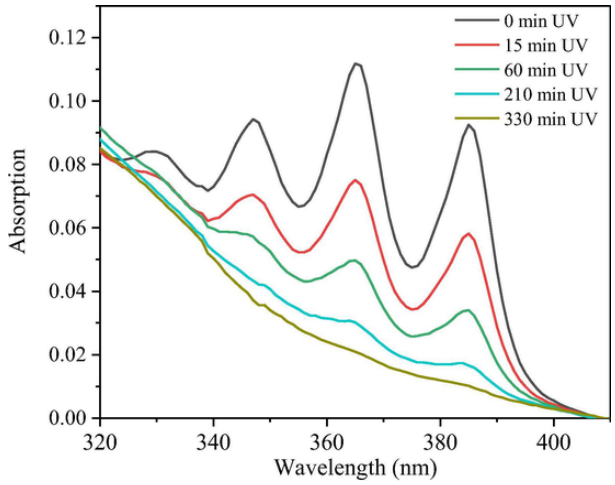

Fig. 4. Decrease of the absorption of **AN**-SiO_2 NPs for various 365 nm exposure times. The initial **AN** concentration was $N_0 = 0.138$ mM.

pendent, as expected since the cross-linking is a bimolecular reaction that proceeds more rapidly at higher **AN** (NP) concentrations.

In order to model the kinetics of the **AN** disappearance, we consider two processes. We take N_{NP} and N to be the concentrations of the NPs and **AN**, respectively. If we take β to be the average number of **AN** molecules per NP, we have $N = \beta N_{NP}$. We assume that the **AN** molecules react as the result of interparticle NP collisions at a rate k_{coll}, leading to a second-order process. Furthermore, we assume that the surface-bound **AN** is also subject to a first-order intraparticle reaction with rate k_1. These assumptions lead to the rate equation

$$\frac{dN}{dt} = -k_1 N - k_{coll} N_{NP}^2 = -k_1 N - k_2 N^2 \quad (1)$$

where $k_2 = \frac{k_{coll}}{\beta^2}$. Eq. (1) can be solved analytically to give

$$N(t) = \frac{N(0)e^{-k_1 t}}{1 + N(0)\frac{k_2}{k_1}\left(1 - e^{-k_1 t}\right)} \quad (2)$$

Note that the N(t) decay depends on the initial concentration N(0) due to the second order term in Eq. (1). We can fit the $N(0) = 0.0125$ mM data in Fig. 5a using Eq. (2). Then, using the values $k_1 = 6.07 \times 10^7$ min^{-1} and $k_2 = 956$ min^{-1} obtained from this fitting, we can plot the predicted N(t) curve for $N(0) = 0.138$ mM. Both the low concentration fit and its high concentration prediction are overlaid with the data in Fig. 5a. The large discrepancy between the experimental and predicted curves for $N(0) = 0.138$ mM shows that a single component model cannot be used to describe the data. If we drop the k_1 term and consider only the second-order k_2 term, the discrepancy becomes even larger.

To achieve agreement with experiment, the theory must take into account the fluorescence decay data that suggests there are at least two different types of **AN** bound to the NP surface, which we denote A and B. If we assume that these populations are subject to different unimolecular decay rates k_{1A} and k_{1B}, we can write a pair of coupled rate equations:

$$\frac{dN_A}{dt} = -k_{1A}N_A - k_2 N_A(N_A + N_B) \quad (3a)$$

$$\frac{dN_B}{dt} = -k_{1B}N_B - k_2 N_B(N_A + N_B) \quad (3b)$$

Here we assume that type A and B **AN** molecules are equally likely to participate in the interparticle dimerization reaction. Also note that k_{1A} and k_{1B} take all intraparticle reactions into account, including dimerization of neighboring **AN**s on a single NP. This is justified by the assumption that the surface-tethered **AN**s cannot diffuse, which leads to first-order kinetics even though this is technically a bimolecular reaction. At time $t = 0$, and given a total initial concentration $N_A + N_B = N(0)$, we define f_A and f_B to be the initial fractions of type A and B molecules, respectively.

$$N_A(0) = f_A N(0) \quad (4a)$$

$$N_B(0) = f_B N(0) \quad (4b)$$

$$f_A + f_B = 1 \quad (4c)$$

The coupled rate Eq. (3) can be solved numerically using a MATLAB computer program. Fig. 5b shows the solutions for $N(0) = 0.0125$ mM and $N_0 = 0.138$ mM, with $f_A = 0.6$, $f_B = 0.4$, $k_{1A} = 0.03$ min^{-1}, $k_{1B} = 0.001$ min^{-1}, and $k_2 = 100$ M^{-1}min^{-1}. These parameters do a reasonable job of reproducing the experimental decays in Fig. 5b.

We can make several comments based on this kinetic analysis. First, it is tempting to associate the 60% of the **AN** population that undergoes rapid decomposition (k_{1A}) with the 80% that undergoes a rapid fluorescence decay. However, this connection is not straightforward because a rapid nonradiative decay process would be expected to compete

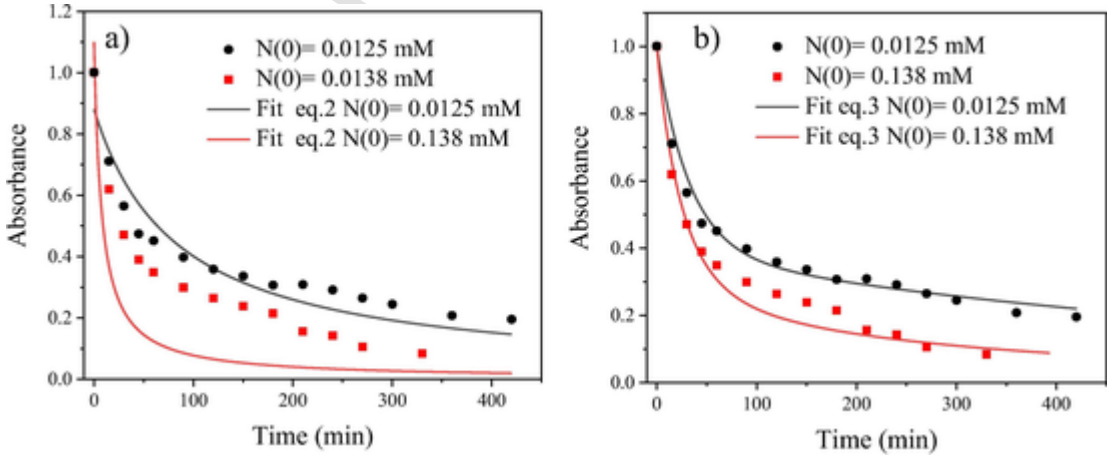

Fig. 5. (a) The time-dependent **AN**-SiO_2 NP absorbance decays overlaid with fits derived using Eqs. (1) and (2) in the text that assume a single unimolecular decay channel with rate k_1. The initial **AN** concentrations ($N(0) = 0.0125$ mM and $N(0) = 0.138$ mM) correspond to different NP concentrations in the suspension, both with the same **AN** surface coverage. (b) The time-dependent absorption decays from Fig. 4b overlaid with fits derived using Eqs. (3) and (4) in the text that assume two different unimolecular decay channels with rates k_{1A} and k_{1B}.

with the unimolecular photochemical reaction rate. It is likely that the rapid nonradiative rate provides a clue that other decay channels (e.g. photochemical reactions) may also be present. The important point is that both reaction rate and fluorescence measurements are consistent with the presence of chemically distinct **AN** populations on the NP surface. Second, this kinetic analysis, which assumes that aggregation is due to interparticle cross-linking, does a reasonable job of fitting the concentration dependent data. One concern we had was that the NP aggregation arose from surface chemistry changes due to intraparticle reactions, rather than interparticle collisions. In this scenario, we would have expected the absorption decrease to be well-described by a single exponential decay reflecting only the unimolecular reaction rate, which is not the case.

Our analysis suggests that a significant fraction of **AN** molecules are lost due to first-order decomposition reactions occurring on the SiO_2 surface. One obvious candidate is photodimerization of two neighboring **AN** molecules on the same particle, although the average distance between **AN** molecules (~1 nm) is substantially larger than the 0.4 nm distance required for this reaction [32]. But there is also evidence that SiO_2 can accelerate the unimolecular photo-decomposition of polycyclic aromatic hydrocarbons and **AN** in particular [33–35]. Unfortunately, there does not seem to be a well-established mechanism for the **AN** decomposition reaction on silica. Surface-mediated reactions with H_2O or O_2 are obvious candidates. From the absorption spectrum of concentrated samples after irradiation, we could identify features associated with the expected products of **AN** oxidation [36] (Supporting Information, Fig. S4). We suspected that the rapid loss of **AN** might be due to an oxidation reaction with O_2 molecules in the liquid but degassing the suspension resulted in an even more rapid loss of **AN** (Supporting Information, Fig. S5). Photoinduced aggregation was also not observed in degassed samples, suggesting that intraparticle decay processes outcompete the dimerization reaction in the absence of O_2. The ability of O_2 to suppress intraparticle **AN** decomposition suggests that the **AN** triplet state may play a role in this reaction. The triplet state, which is known to undergo electron transfer reactions [37,38], has not been considered previously as a culprit in the decomposition of **AN** on SiO_2.

Finally, we analyzed the kinetics of the interparticle photodimerization cross-linking reaction. Given the rate $k_2 = 100\ M^{-1}min^{-1}$, and $\beta = 1100$, we obtain the experimental $k_{coll} = 2 \times 10^7\ M^{-1}s^{-1}$. k_{coll} can also be calculated using the Smoluchowski bimolecular reaction rate given by [39]

$$k_{coll} = 4\pi D R_{react} \tag{5}$$

where D is the diffusion constant of the NP and R_{react} is the reaction radius. The Stokes-Einstein equation for D is

$$D = \frac{k_B T}{6\pi\eta R} \tag{6}$$

where k_B is the Boltzmann constant, T is the temperature, η is the viscosity, and R is the particle radius. If we assume the reaction and particle radii are identical, $R = R_{\mathrm{react}}$ and we have

$$k_{react} = \frac{2}{3}\frac{k_B T}{\eta} \tag{7}$$

Plugging in $T = 298$ K and $\eta = 0.89$ centipoise, we calculate $k_{coll} = 3.1 \times 10^{-12}\ cm^3/s = 1.8 \times 10^9\ M^{-1}s^{-1}$. This value is about 100 × larger than the experimental k_{coll}. The lower experimental rate is not surprising, since the cross-linking reaction requires a photoexcited **AN** molecule to be correctly oriented with respect to an **AN** molecule on the other NP during the collision. This analysis shows that the NP photocross-linking reaction is far from diffusion-limited, consistent with previous results on photoinduced noncovalent aggregation [11].

From our analysis of the NP cross-linking kinetics, it is clear that the photoinduced assembly of silica NPs provides several opportunities for improvement. First, there exist at least two different reaction pathways on the NP surface that compete with the desired interparticle dimerization. This is not too surprising: the important role of SiO_2 surface heterogeneity has been recognized in a variety of chemical processes [40–42]. An improved knowledge of the SiO_2 surface and **AN** binding sites is probably necessary to identify chemical modifications that can prevent these side reactions. Alternatively, a more robust photochemical cross-linking agent might avoid these side reactions altogether. Second, the efficiency of the interparticle reaction after collision is estimated to be on the order of 1%. Improving interparticle reactivity, for example by lengthening the **AN** tethering chain, might improve the yield of this reaction. Elimination of the non-productive intraparticle reactions and optimization of the desired interparticle reaction should increase the photoinduced assembly rate by at least one order of magnitude.

4. Conclusion

From a practical standpoint, the results of this paper demonstrate that photodimerization of surface **AN**s can be used to cross-link SiO_2 NPs. However, this reaction exhibits fairly complicated kinetic behavior, with at least two different intraparticle decomposition pathways that compete with the interparticle cross-linking photodimerization. Although SiO_2 is often considered to be chemically inert, its surface heterogeneity can provide environments that enhance the photodecomposition of surface-bound **AN**. In order to utilize the SiO_2 surface as a robust platform for organic photochemistry that leads to photoresponsive nanomaterials, a clearer understanding of how its heterogeneous nature affects photochemical reactions will be necessary. We hope that the kinetic model developed here will prove useful in analyzing future experiments.

CRediT authorship contribution statement

Seyed Hossein Mostafavi: Data curation, Formal analysis, Investigation, Writing - review & editing. **Magi Mettry:** Investigation. **Adam David Gill:** Investigation. **Connor J. Easley:** Investigation. **Richard J. Hooley:** Supervision, Funding acquisition. **Christopher J. Bardeen:** Conceptualization, Supervision, Writing - original draft, Project administration, Funding acquisition.

Declaration of Competing Interest

The authors declare that they have no known competing financial interests or personal relationships that could have appeared to influence the work reported in this paper.

Acknowledgements

The authors thank the National Science Foundation (DMR-1810514 to C.J.B. and CHE-1708019 to R.J.H.) for support.

Appendix A. Supplementary material

Supplementary data to this article can be found online at https://doi.org/10.1016/j.cplett.2019.137059.

References

[1] A.C. Balazs, J. Aizenberg, Soft Matter. 10 (2014) 1244–1245.
[2] C. Cardenas-Daw, A. Kroeger, W. Schaertl, P. Froimowicz, K. Landfester, Macromol. Chem. Phys. 213 (2012) 144–156.
[3] X. Yuan, K. Fischer, W. Schartl, Adv. Func. Mater. 14 (2004) 457–463.
[4] X. Yuan, K. Fischer, W. Schartl, Langmuir 21 (2005) 9374–9380.
[5] X. Yuan, M. Schnell, S. Muth, W. Schartl, Langmuir 24 (2008) 5299–5305.
[6] J. Zhou, R. Sedev, D. Beattie, J. Ralston, Langmuir 24 (2008) 4506–4511.
[7] S. Pocoví-Martínez, M. Parreno-Romero, S. Agouram, J. Perez-Prieto, Langmuir 27 (2011) 5234–5241.

[8] J.W. Chung, K. Lee, C. Neikirk, C.M. Nelson, R.D. Priestley, Small 8 (2012) 1693–1700.
[9] P.J. Roth, P. Theato, Macromol. Chem. Phys. 213 (2012) 2550–2556.
[10] Y. Chen, Z. Wang, Y. Hea, Y.J. Yoon, J. Jung, G. Zhang, Z. Lin, Proc. Nat. Acad. Sci. 115 (2018) E1391–E1400.
[11] C. Zhou, Y. Zhao, T.-C. Jao, C. Wu, M.A. Winnik, J. Phys. Chem. B 106 (2002) 9514–9521.
[12] N.S. Bell, M. Piech, Langmuir 22 (2006) 1420–1427.
[13] R. Klajn, K.J.M. Bishop, B.A. Grzybowski, Proc. Nat. Acad. Sci. 104 (2007) 10305–10309.
[14] A. Kimoto, K. Iwasaki, J. Abe, Photochem. Photobiol. Sci. 9 (2010) 152–156.
[15] A. Kohntopp, A. Dabrowski, M. Malicki, F. Temps, Chem. Commun. 50 (2014) 10105–10107.
[16] Y. Shiraishi, E. Shirakawa, K. Tanaka, H. Sakamoto, S. Ichikawa, T. Hirai, Appl. Mater. Interf. 6 (2014) 7554–7562.
[17] Y. Lan, Y. Wu, A. Karas, O.A. Scherman, Angew. Chem. Int. Ed. 53 (2014) 2166–2169.
[18] H. Zhao, S. Sen, T. Udayabhaskararao, M. Sawczyk, K. Kučanda, D. Manna, P.K. Kundu, J.-W. Lee, P. Král, R. Klajn, Nat. Nanotech. 11 (2016) 82–88.
[19] G.-M. Andres, J. Perez-Juste, L.M. Liz-Marzan, Adv. Mater. 22 (2010) 1182–1195.
[20] X. Wang, J. Feng, Y. Bai, Q. Zhang, Y. Yin, Chem. Rev. 116 (2016) 10983–11060.
[21] A.R. Smith, D.F. Watson, Chem. Mater. 22 (2010) 294–304.
[22] Q. Zhou, B. Zhang, D. Han, R. Chen, F. Qiu, J. Wu, H. Jiang, Chem. Commun. 51 (2015) 3124–3126.
[23] H.-S. Jung, J.-K.L. Doo-SikMoon, J. Nanomater. (2012) 593471/593471-593478.
[24] M. Mazur, G.J. Blanchard, Langmuir 21 (2005) 1441–1447.
[25] M. Nakamura, M. Shono, K. Ishimura, Anal. Chem. 70 (2007) 6507–6514.
[26] I.-L. Hsiao, S. Fritsch-Decker, A. Leidner, M. Al-Rawi, V. Hug, S. Diabaté, S.L. Grage, M. Meffert, T. Stoeger, A.S. Dagmar Gerthsen, C.M. Ulrich, C.W. Niemeyer, Small 15 (2019) 1805400/1805401-1805411.
[27] R.P. Bagwe, L.R. Hilliard, W. Tan, Langmuir 22 (2006) 4357–4362.
[28] C. Graf, Q. Gao, I. Schütz, C.N. Noufele, W. Ruan, U. Posselt, E. Korotianskiy, D. Nordmeyer, F. Rancan, S. Hadam, A. Vogt, J.R. Lademann, V. Haucke, E. Rühl, Langmuir 28 (2012) 7598–7613.
[29] Y.S. Liu, W.R. Ware, J. Phys. Chem. 97 (1993) 5980–5986.
[30] H. Wang, J.M. Harris, J. Phys. Chem. 99 (1995) 16999–17009.
[31] D. Roy, S. Piontek, R.A. Walker, 13 (2011) 14758–14766.
[32] V. Ramamurthy, K. Venkatesan, Chem. Rev. 87 (1987) 433–481.
[33] S.P. Zingg, M.E. Sigman, Photochem. Photobio. 57 (1993) 453–459.
[34] R. Dabestani, K.J. Ellis, M.E. Sigman, J. Photochem. Photobiol. A 86 (1995) 231–239.
[35] M. Mazur, G.J. Blanchard, J. Phys. Chem. B 108 (2004) 1038–1045.
[36] H. Fidder, A. Lauer, W. Freyer, B. Koeppe, K. Heyne, J. Phys. Chem. A 113 (2009) 6289–6296.
[37] J.-S. Hsiao, S.E. Webber, J. Phys. Chem. 96 (1992) 2892–2901.
[38] D.R. Worrall, S.L. Williams, F. Wilkinson, J. Phys. Chem. B 101 (1997) 4709–4716.
[39] E.A. Mun, C. Hannell, S.E. Rogers, P. Hole, A.C. Williams, V.V. Khutoryanskiy, Langmuir 30 (2014) 308–317.
[40] B.A. Morrow, A.J. McFarlan, J. Phys. Chem. 96 (1992) 1395–1400.
[41] Y. Kholin, V. Zaitsev, Pure Appl. Chem. 80 (2008) 1561–1592.
[42] A.M. Schrader, J.I. Monroe, R. Sheil, H.A. Dobbs, T.J. Keller, Y. Li, S. Jain, M.S. Shell, J.N. Israelachvili, S. Han, Proc. Nat. Acad. Sci. 115 (2018) 2890–2895.